Ayoub Moradi[1]

[1]Iranian Space Research Center.

Corresponding author: Ayoub Moradi (ayoubmoradi@gmail.com)

Key Points:

- An analytical destriping method is developed to optimize a Poisson filter based on spatial contrast of the signal.
- Using this method a set of space-time variable dynamic filter can be designed which allow to enhance local signals, leading to reduce total errors.
- The optimal Poisson filters length for the Caspian Sea and Congo River Basin are 400km and 550km respectively.

Abstract

In the result of uneven density of data acquisition, satellite gravimetry level-2 data suffer from global north-south stripping. By applying various filtering methods, several studies have been involved in data destriping. However, the studies mainly deliberated the question in the global scale, and local impacts are not considered. In other hand, water studies, in particular inland hydrology, mostly deal with small scale figures such as lakes and watersheds. Therefore, the local data destriping methods need special attentions. This research presents a new analytical method to de-stripe gravimetry data based on spatial contrast of signals. The approach makes a balance between destriping and signal preservation. Utilizing a priori information extracted from the gravimetry data itself, the destriping method first estimates the spatial gradient of signal, and based on that, it optimizes a Poisson filter to de-stripe the data. Unlike the other approaches, the optimized filter is dynamic taking into account time variations of signal contrast such as seasonality. The proposed approach is applied on ten globally distributed study areas in order to derivate general regulation. Detailed process and the evaluations are applied on two of the study areas: the Caspian Sea and the Congo River Basin. The results are visually evaluated for spatial fitting, and evaluated for temporal consistency by comparing to outcomes of other filters. Use of a dynamic filter set specified for any region and time, allows to highly preserve local hydrological signals which are vulnerable to globally optimized filters. It also allows to effectively constrain filter-induced errors.

1 Introduction

The main text should Accurate estimation of the continental water storage changes is important in many domains. Spatial observation and monitoring of the Earth's hydrosphere by remote sensing came back to the 1970s. However, with the emergence of Gravity Recovery and Climate Experiment (GRACE) mission in 2002, this domain experienced an unprecedented progress. Satellite gravimetry serves various domains including: sea level studies (Willis et al., 2008; Schrama & Wouters, 2011; Jacob et al., 2012; Feng et al., 2012; Peng et

al., 2013; Joen et al., 2018), hydrological processes (Zhong et al., 2009; Feng et al., 2013; Guo et al., 2016), ground water storage variations, draught (Chen et al., 2009), oceanography (Johnson & Chambers, 2013; Piecuch et al., 2013), and, glaciers (Chen et al., 2007; Luthcke, 2008; Luthcke et al., 2008; Velicogna, 2009; Jacob et al., 2012; Sasgen et al., 2012; Barletta et al., 2013; Gardner et al., 2013; Velicogna et al., 2014; Sorensen et al., 2017). Satellite gravimetry presents the geoid topography data with respect to a reference date. The gravity time variations are mainly caused by Earth's mass redistribution (Swenson and Wahr, 2002), load induced surface deformations, postglacial isostasy rebound, and oceanic and atmospheric tides. The solutions are corrected for tides prior to gravity field estimation (Tapley, 2004; Bettadpour, 2007). The time variable part of the geoid changes is usually considered to be associated with the change in vertically integrated water content. The Equivalent Water Height (EWH) may be retrieved with an accuracy of less than 1 cm over a large area. However, the accuracy decreases for small scale studies depending on processing and the applied filter.

The gravimetry derived signal is reliable particularly where either a big signal to noise ratio exists, either the study area is large enough to sustain resolution. The signal is thus sensitive to spatio-temporal smoothing when dealing with small study areas. GRACE estimates are normally erroneous due to measurement noise and the aliasing induced by high-frequency mass variations (Swenson and Wahr, 2002; Wahr et al., 1998; Swenson and Wahr, 2006). The most known errors in satellite gravimetry data, is the globally dominant stripe-like correlation error, known also as commission error (Gunter et al., 2006). The stripe-like error, is a consequent of aliasing and limitation in data acquisition. Due to the polar orbiting platform, stripe error shows a north-south pattern on the Earth (Tapley et al., 2004). It originates from, but not limited to, the imperfections in the reference gravity field model used in the estimation process. Cerrorelation error is unevenly distributed across SH components, increasing rapidly with Spherical Harmonic Truncation (SHT) degrees.

Different methods for signal decorrelating are developed. The methods are considered in different point of view in literature; and they are thus differently classified. Based on similarities, we summarized the methods in two general categories. Category one: empirical or statistical filters which deal with the error as a systematic and deterministic contribution (e.g.: in Wahr et al., 1998; Swenson and Wahr, 2006; Wouters and Schrama, 2007). These filters need the assumption that the noise contribution in total signal is already known by the user. The empirical filters relay on distinguishing between spatially correlated error and variant signal. They briefly functions as follow: the correlation error is approximated through an optimal polynomial fitting within a moving window over SH coefficients of each order but same parity (i.e.: even or odd degrees separately). Estimated correlation error is finally subtracted from the total signal, remaining decorrelated signal. The empirical filter is more effective in middle to higher latitudes; whereas, it is inefficient in equatorial regions. The empirical filter may differ based on the approach used for the polynomial approximation:

the same polynomial fitting may be applied to the entire SH series (such as in Chambers, 2006; Ferreira et al., 2012). Otherwise, local polynomial approximation may be employed on interested subsets. In the other hand, the window length can vary in spectral domain: the same window length for all coefficients. Either, an order-dependent window length (e.g.: in Swenson & Wahr, 2006) may be applied.

The category one has been widely used due to its simplicity and low inputs. The Gaussian filter is most common and frequently used filter of category one. Gaussian smoothing has been the standard method in the early exploitation of GRACE products, due to its ease in implementation and intuitive interpretation (Wahr et al., 1998). The isotropic Gaussian filter was first formulated by Jekeli (1981) in physical geodesy. This filter attenuates the power of high-frequencies which are represented as high degree and order spherical harmonic coefficients in the gravity field. Swenson and Wahr (2006) proposed a low order polynomial fitting on a moving window. Piretzidis and Sideris (2018) designed an integrated software to apply empirical decorrelation on GRACE SH, named SHADE (Spherical HArmonic coefficient empirical DE-correlation). The downside of this approach is that it does not accounts for the variable data density that increases towards the poles. As the correlation noise varies with both degree and order, anisotropic Gaussian filter demonstrated better efficiencies Han et al. (2005).

Category two: data driven, analytical filters which account for the error as combination of systematic and stochastic components (e.g. in: Kusche, 2007; Klees et al., 2008; Kusche, 2009; Horvath et al., 2018). The fundamental difference with the category one, is the necessity to employ additional knowledge about the signal, known as *a priori* information, instead of the assumption which is principal in the filters of category one. Although, few studies (e.g.: Klees et al., 2007) developed a regional hydrological model to exploit as *a priori* information about mass variations; however, most of the studies (e.g: Sasgen et al., 2006; Kusche, 2007; Kusche et al., 2009) utilized the characteristics of the GRACE spherical harmonic coefficients for this purpose. Use of, e.g.:, the characteristics of the GRACE spherical harmonic coefficients (e.g: Sasgen et al., 2006a; Sasgen et al., 2006b), these filters employ the covariances of signal and noise to optimize the signal. Kusche (2007) exploited the estimation of GRACE tracking as a priori information. Kusche (2007) provided a priori information by the estimation of GRACE tracking using a Bayesian regularization over spherical harmonic coefficients (Koch and Kusche, 2002; Kusche, 2007). As anisotropic method, which is more efficient than conventional Gaussian isotropic filters, Kusche et al. (2009) introduced so-called DDK filter. This filter is simplified version of the Kusche-2007 filter. The GRACE error covariance matrix used in the construction of the decorrelating kernel in Kusche method, is created synthetically, using one month of GRACE twin-spacecraft orbits and a simplified method for mapping the K-band inter-satellite ranging observations into the spherical harmonics. The primary (Kusche, 2007) method employed a full filter matrix as large as SH coefficients. However, the simplified version (Kusche,

2009) is generalized to the order-only convolution (comparable to the approach in Swenson and Wahr (2006)), facilitated its usage by a wider community of users of GRACE products. Kusche et al. (2009) applied DDK filter on GRACE RL04 monthly gravity from GFZ solutions, resulting good agreement with mass anomalies derived from a global hydrological model. Lorenz (2009) presented a regularization method for applying on the signal and error covariance. This approach latterly further developed by Devaraju et al. (2016), and Devaraju and Sneeuw (2017). By using an energy integral method, Seoane et al. (2013) developed a regional GRACE solutions from 2003 to 2011over Australia. This approach uses the dynamical orbit analysis of GRACE Level 1 measurements, and especially accurate along-track K-band range rate (KBRR). It reduction of GRACE Aliasing errors.

DDK series are the most known filters of category two. Their efficiency is (e.g.) demonstrated on the globally gridded monthly terrestrial water storage variations are provided by ICGEM GFZ (Zhang et al., 2016; Dahle et al., 2012). In this series, the signal variance and error covariance matrices are derived from geophysical models and the GRACE orbit data respectively. However, GRACE orbit data of August 2003 are used as static for the entire time series. It thus, does not account for time dependent variations in geophysical signal contents. More recent studies (e.g.: Horvath et al., 2018) attempted to overcome this shortage of DDK series by introducing time variable data driven approaches named VADER filter. Unlike DDK filter, VADER exploits GRACE level2 error covariance information by the total time series. Consequently, this filter accounts for seasonality in geophysical signal content. The VADER filter achieved an improvement of 15% in reduction of cumulative geoid height errors. It also obtains better destriping and delivers smaller formal errors comparing to static filters like the DDK filter (Horvath et al., 2018).

In general, spatial smoothing decreases the stripe-like noises (Wahr et al., 2006; Swenson and Wahr, 2006), however, reducing the signal, it introduces itself a distortion (Wahr et al., 1998a, b; Landerer and Swenson, 2012). This distortion is called as either leakage, or bias in literature (e.g. Wahr et al., 1998; Swenson and Wahr, 2002; Swenson et al., 2003; Klees et al., 2007; Tang et al., 2012; Zou and Jin 2014; Zhang et al., 2015; Jin and Zou 2015; Joen et al., 2018). Large study areas, taking as a total, suffer from small distortion effects; however, the signal would fade in small study areas. The destripping has been the subject of many studies attempting to minimize the total global error. However, it is still a challenging process in gravimetry society; in particular, the efficiency of destriping methods are not assessed for small-scale signal retrieving. In the case of satellite gravimetry, *a prior* information are not easily available. In this study, we investigate the filtering effects from the first category, focusing on the isotropic Poisson filter. The primary goal of this study is investigating the optimal Poisson filter to preserve local signals.

2 Materials

The current study is based on the middle latitudes; however, few cases in lower

and higher latitudes are also investigated. We chose ten study units (Figure 1), seven of which are located between 35 N and 53 N. Five units are over the lands, and two units over the oceans. Out of the middle latitudes, two study units are selected in Canada. This region is known for large mass variations, as well as, for large land-ocean leakage effects. Located around the Equator, the last study unit is the Congo River basin. The study units from east to west are entitled as: Atlantic (Atl), Wyoming (WY), Kansas (KS), North-Western Passages (NWP), Baffin Bay (BfB), Pacific (Pac), Congo River basin (Cg), Caspian Sea (CS), Bukhara in Uzbakistan (Uz) and Xinjiang in China (Xin).

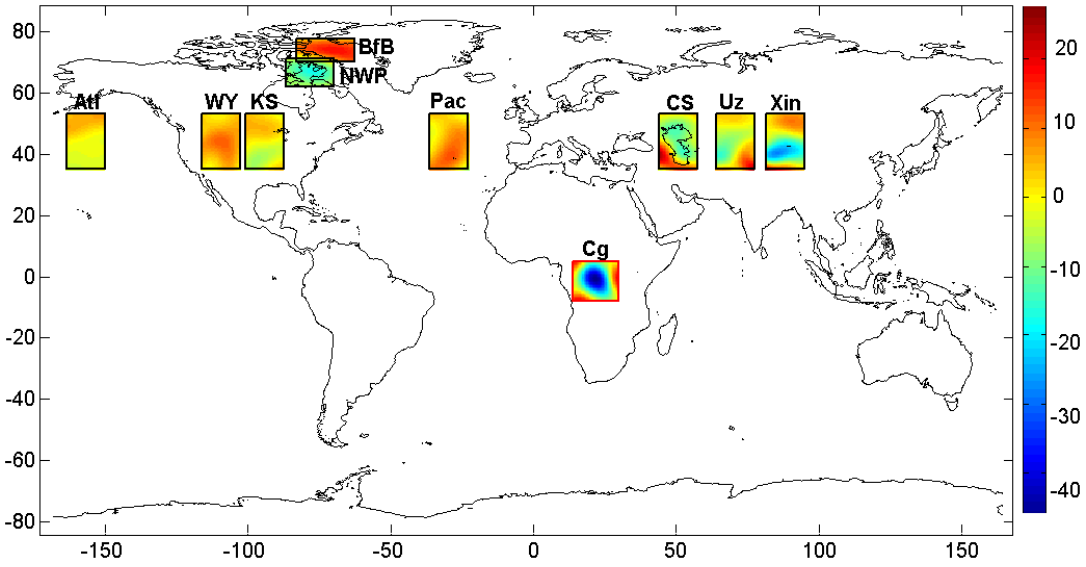

Figure 1. Situation of the study areas.

In this study two categories of data are utilized: 1) gravimetry data for estimation of optimized filter bandwidth, and for evaluation of the filter function; and 2) non-gravimetry data for analysis of seasonal contrast. We used the GRACE level-2 SH normalized solutions from JPL (Jet Propulsion Laboratory) over 2004-2014 to estimate mean annual signal contrast. In order to evaluate the filer efficiency, we exploit gravimetry solutions from AIUB (Astronomical Institute University Bern) applying DDK series filters; as well as, gravimetry solutions from CNES/GRGS which are already stabilized and corrected for high frequency mass variations (Thompson et al., 2004, and Lemoine et al., 2013). GRGS and AIUB Analysis Centers are selected based on its long-term experiences on providing stabilized GRACE data and associated products. The GRGS solutions include the second (G02) and third (G03) releases truncating respectively at SH degree maximal of 50 and 80, are used. The monthly G03 data benefits from improved spatial resolution, however, the G02 solutions are based on the 10-days maximum value, giving denser time sampling. Among the study areas CS and Cg include considerable seasonality in water mass fluctuations.

Space borne altimetry provides direct measurements of the Caspian Sea water level. We benefit from satellite altimeter passes over the Caspian Sea as independent measurements to evaluate the CS seasonal fluctuation derived from gravimetry data. In the sea level studies, the measurements are ideal to reach an accuracy of 3.4 cm or better (J-2 Handbook). We employed a set of satellite altimetry data with accuracy rates within the specified optimal accuracy. The accuracy of Jason-1 altimeter (by NASA/ CNES) is estimated to be 3.3 cm by JPL, and 2.5 cm by CNES (Gourine, 2013). The Jason-2 altimeter accuracy is estimated to be about 2.5 cm in Jason-2 documentation (by JPL), and 2 cm by CNES (Gourine, 2013). The seasonal contrast of water mass in the Congo River Basin are analyzed by long-term river discharge data provided from The Center for Sustainability and the Global Environment, SEGA (Wisconsin, 2011). Specification of data are summarized in Table 1.

Table 1. Description of data used

Source	Data	Data span	Resolution	Filtering			
		From	To	spatial*	Temporal	spatial	temporal
GRACE	JPL RL06	2004	2014	SHT: 60	Monthly		
	GRGS RL02	2004	2014	SHT: 50	10 days		
	GRGS RL03	2004	2014	SHT: 80	Monthly		
	AIUB-DDK1	2004	2014	SHT: 96	Monthly		
	AIUB-DDK4	2004	2014	SHT: 96	Monthly		
	AIUB-DDK7	2004	2014	SHT: 96	Monthly		
Jason 1	SSALTO	2001	2013	176 cycles	10 days		
Jason 2	SSALTO	2008	2017	573 cycles	10 days		
river disch.	FGGE	2000	2015	2 stations	Monthly		

*Spatial resolution is defined by the Spherical Harmonic Truncation (SHT)

3 Filter optimization

In gravimetry derived time series of EWH, the effect of stripes is revealed as large RMS on high resolved inversions (i.e. in high SHT), and small RMS on low resolved inversions (i.e.: in low SHT). Independent of study area, spatial filtering follows a general pattern: in small filter lengths the estimations are very different, with high RMSs, giving large estimations for large SHTs and small estimations for small SHTs. With increase in filter length, both the amplitudes and RMSs of estimations proportionally decreases (i.e.: larger SHTs decrease more), leading to all the estimations be approaching. Beyond a specific filter length, the amplitude decreasing effect of the filter dominates the RMS decreasing effect (Figure 2). This limit corresponds to the optimum filter length for the signal of interest. Filtering by a filter length smaller than the optimum limit leads to remaining the stripes; and over-filtering makes the estimations smoothed, fading spatial variability. Therefore, the filter efficiency is determined by the minimizing rate of the RMS of difference for selected SHTs (SHTs >40 in our

case), and the preserving rate of the mean amplitude of estimation, as Equation 1. Filter efficiency for different filter lengths are shown in the Figure 2:

Minimize the RMS of difference

Filter efficiency = 1/ RMS * Amp. (1)

Preserve the amplitude of estimations

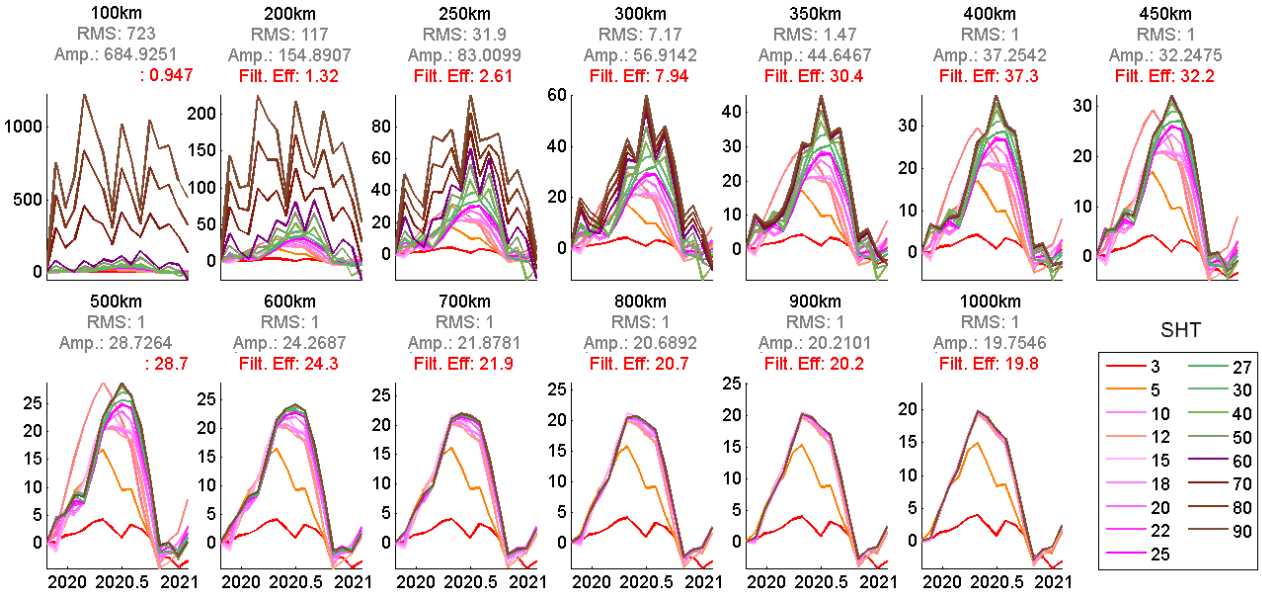

Figure 2. Estimated signal after different truncations and different filtering (for the CS).

The estimations derived from filter length and SHT of regular intervals (50km and 3degree respectively) illustrates obviously the optimum filter length. In the case of Caspian Sea (Figure 3), the normalized integral signal reaches zero at the filter length of 400 km. Note that, the small SHTs (smaller than 20 in this case) are not highly affected by stripes; that is the reason that the signal integration does not change with filter length increase.

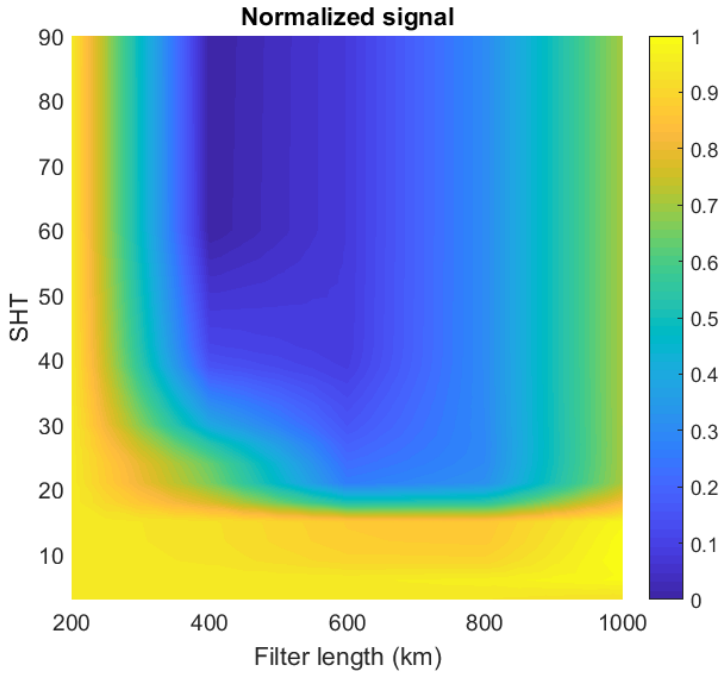

Figure 3. Filter-SHT Matrix of signal for truncations by 1:3:90, and filtering by 200:50:1000 km.

Considering that the decreasing downward RMS leads to minimize the integration of estimations, and according to the Filter-SHT matrix, the optimum filter can be expressed as follow:

$$\text{Filt.Opt} = \min\left(\sum_{\text{SHTa}}^{\text{SHTb}} \text{Es.}\right) \quad (2)$$

which Es is the estimation of signal for truncations from 'a' to 'b'.

The Equation 2 corresponds to the sum of columns in the Filter-SHT Matrix. The Filt.Opt depends on SHT, decreasing in a cotangent-like form; however, it is independent of signal amplitude, because the signal amplitude does not change the signal scattering pattern (see Appendix A). Therefore, the Filt.Opt is independent of signal velocity in time; it depends however on signal gradient in space. Supposing that, an -imaginary- displacement in the X axis of the Filter-SHT Matrix would cause a change in Filt.Opt, any change in spatial dimensions of the signal also makes a change in the Filt.Opt. In the other word, for specifying the Filt.Opt, it is not important how much the signal amplitude is large, instead, it is important how much the signal is spatially sloped. A steep signal is better distinguished from adjacent signals, allow it to be enhanced with a weak filter, and inversely, a plain or low-sloped signal needs stronger filters to recover. The roof value for expanding the Filt.Opt is limited by the GRACE(FO) spatial resolution: meaning that, the maximum Filt.Opt for a low

sloped signal (e.g.: over the Oceans) is limited by the GRACE(FO) resolution, which depends on the latitudes. Because, any homogenous signal within a scale of 2X2 imaginary pixel is ensured to be captured as, at least, by one imaginary pixel of the GRACE(FO). The gradient (or slope) is considered from the center of study unit outwards; by (Equation 3). Specified Filt.Opt based on the signal spatial gradients, for all study units are shown in Figure 4. And, the relationship of the Filt.Opt and the signal gradients are shown in Figure 5.

$$\text{Slope} = \tan\left(\frac{\text{dSig(mm)}}{\text{dx(km)}}\right) \quad (3)$$

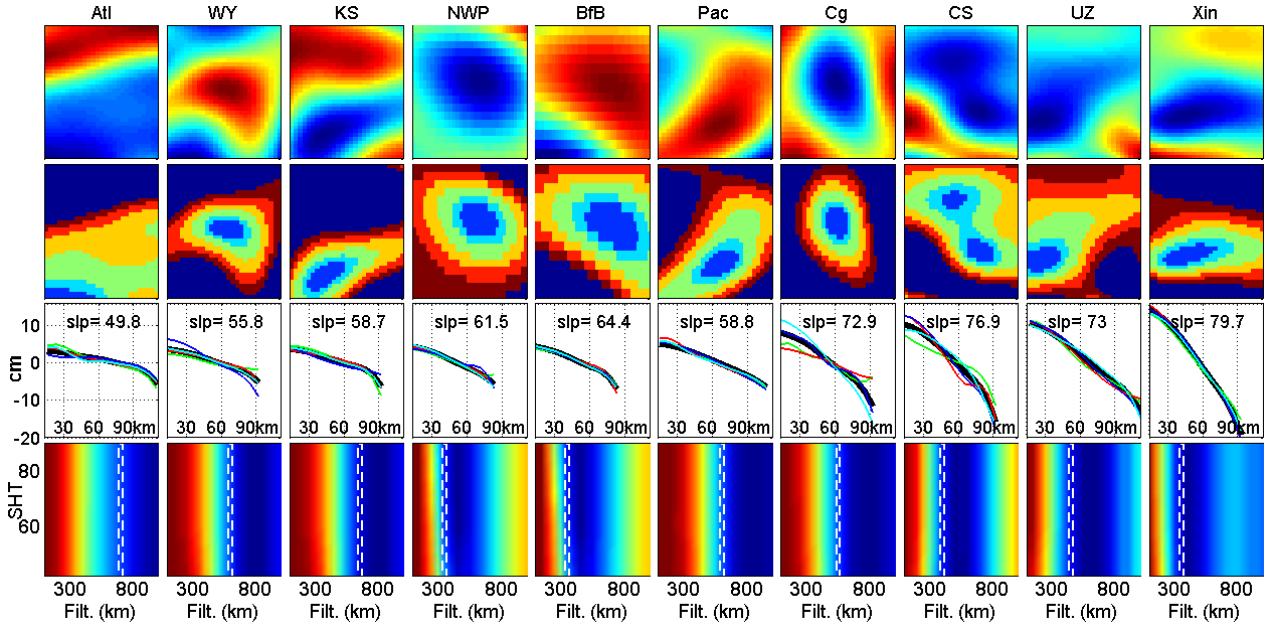

Figure 4. First row: the signal; second row: buffering; third row: spatial gradient; fourth row: Filter-SHT Matrices with the column of minimum marked by dashed white lines.

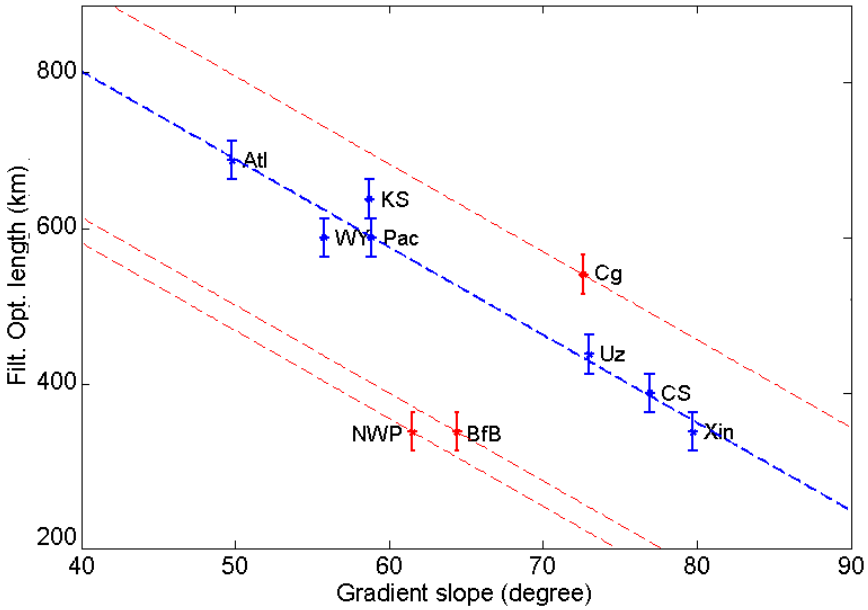

Figure 5. Relationship between Filt.Opt and signal spatial gradient

The relationship between gradient slope and Filt.Opt of the study areas indicates on a strong correlation for the units located in the same latitude. However, NWP and BfB show smaller Filt.Opt, and Cg, shows larger Filt.Opt than the linear regression estimated for mid-latitudes. These biases are associated to the background stripping density, which increases toward the Equator and decreases toward the poles. The optimal filter length is thus, defined by the spatial gradient of signal plus a background factor which varies latitudinally (Equation 4). The latitudinal effect has a tangent-like pattern; i.e.: it decreases about 20% from Equator to ±70 degrees, and rapidly decreases beyond ±70 degrees (Equations5). This is why comparing to Cg study area, the Filt.Opt of NWP and BFB are more different to the predictions for mid-latitude, while they are latitudinally closer. Equation 6 is developed to project the tangent-like (0-to-∞) pattern in 0-to-1.

Filt.Opt $\Rightarrow f(signal\ gradient,\ background\ stripe, latitude)$ (4)

Filt.Opt= [-1* (*slope*) + *L*]*10, (5)

L= -125*((tan (*Lat*)/ tan (89)) ^0.5*-1+1) (6)

Depending on the stripe intensity variations, L may also vary partially in time. The variations are random, however small enough allowing, for example, to exploit a static one-month orbital information as *a priori* to minimize stripes over long periods (e.g.: in DDK filters). For the period of study, the monthly mean-removed stripes include a Standard Deviation of 6.4% relative to the mean.

3.1 Seasonal variations in optimal filter

Although the Filt.Opt is independent on time in terms of signal amplitude, it may depend on time for spatial gradient. Altimetry driven water level variations in CS and long-term water balance of the Cg show the most difference between spring/winter and summer/autumn in the CS, and the most difference between autumn/winter and spring /summer in the Cg (Figure 6). Examination with seasonal combinations of GRACE data also confirm the seasonality in CS and Cg (Figure 7). The seasonal differences in spatial slope cause a difference in Filt.Opt in the order of 10 meters.

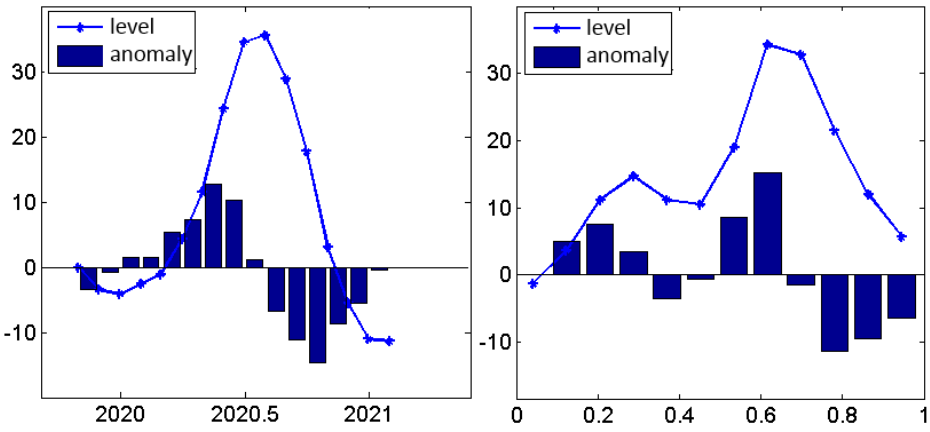

Figure 6. Water balance pattern of the CS in 2020 (left), and long-term mean of the Cg (right).

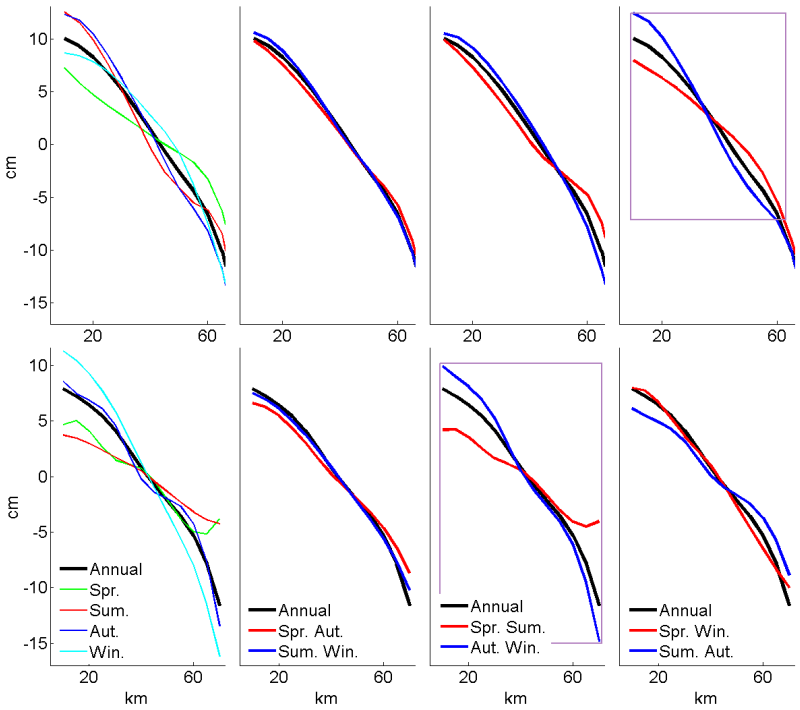

Figure 7. Seasonal variations in signal spatial gradient in the CS (upper row) and the Cg (lower row). Differences are ten times magnified for better illustrations.

3.2 Analysis of sensitivity to filter length

In order to investigate the sensitivity to filter length, and thus, the importance of filter optimization, the signal variances over a 1000km-range filter length is analyzed for a sample date (March 2014). The signal variances resulted from 19 filters (100:50:1000 km) is composed using the Principle Component Analysis (PCA) method. This method concentrates the variances in constructed figures ranked from 1st to nth. There is a high correlation coefficient (0.796) between the original signal amplitude and the filter-induced variance derived from the first component of PCA (Figure 8). It mean that where the signal is large and spatially sloped (regardless to the sign), it is more sensitive to filter length. Note to not confuse the dependency of signal amplitude and sensitivity to filter, with the independency of signal amplitude and

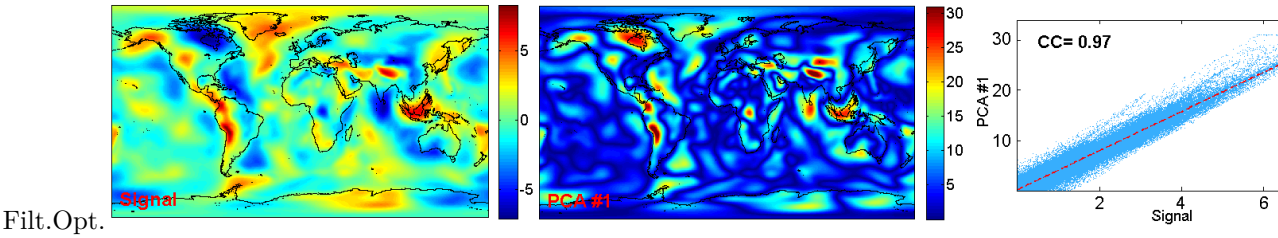

Filt.Opt.

Figure 8. Left: map of the original signal; Middle: PCA #1 of the filter set (100:50:1000); and, Right: correlation between the two maps.

4 Evaluation of the optimized filter

In this section, the results are evaluated temporally and spatially. As well as, the seasonal efficiency of filters are evaluated. For the spatial evaluation, the EWH maps derived with different filter length applied, are visually checked. The example maps are shown for CS and Cg study areas in Figure 9. The maps indicate on the best fits on 400km and 550km filter lengths for CS and Cg respectively, particularly in high SHTs.

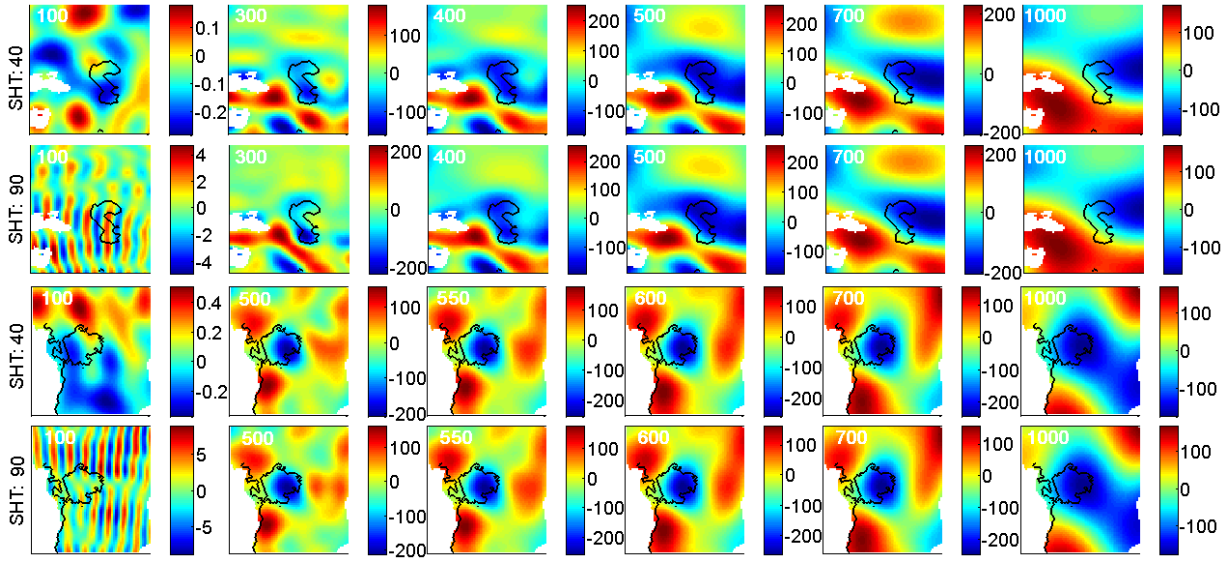

Figure 9. Visual comparison of filter length effects over the CS (2 upper rows) and Cg (2 lower rows).

For the temporal evaluation of the results, EWH are estimated from the solutions applying different filters, and all series are corrected for leakage effects in the same approach. The estimations are compared in Figure 10. The solutions processed by AIUB with applying a DDK series are based on data constraining via *a priori* information derived from one month orbit data (August, 2003). However, as it is already mentioned, the GRGS solutions are already stabilized

by the distributer and thus does not need filtering. As shown in Fig. 10, the Poisson 400km filtering is highly consistent to the GRGS Releases and to the DDK-7. Three mentioned time series include lower corrections with strong DDK filters, especially with DDK-1.

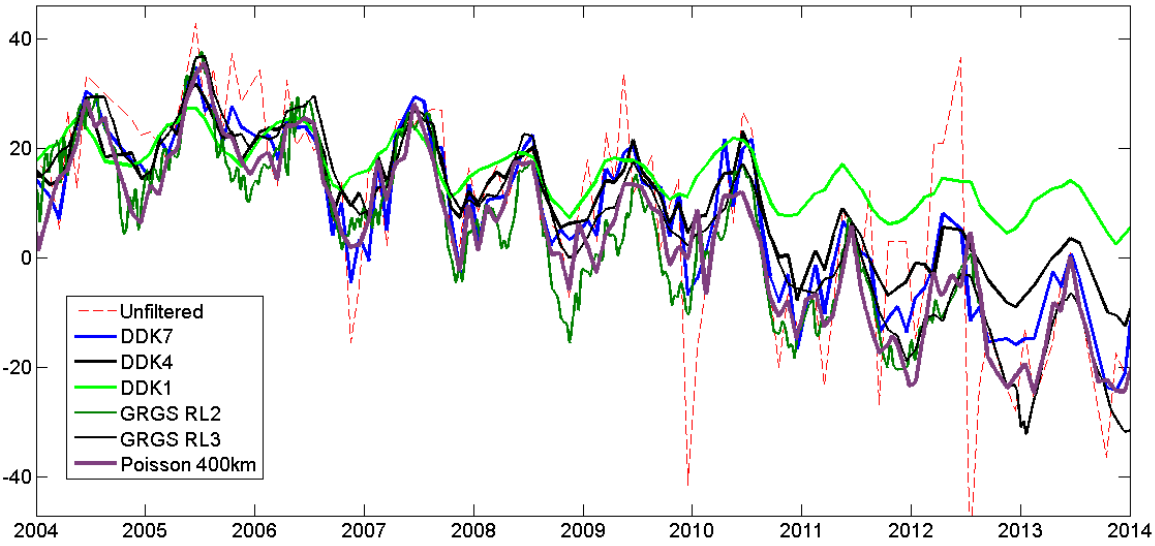

Figure 10. Comparison the time series filtered by the Poisson 400km, DDK series and GRGS filtering methods.

In order to evaluate the efficiency of seasonally different filter lengths, the results of different filter combinations are analyzed. Corresponding to the signal gradient, a set of 10km-interval filters is applied on the CS and Cg study areas. Altogether, 21 and 10 filter combinations are examined on CS and Cg respectively. The best RMS improvements are obtained from the applying of a 370-400 km and a 530-560 km filter lengths for the CS and Cg respectively (Figure 11). In examinations the smaller filter is applied on the season of higher gradient and the larger filter is applied on the season of lower gradient. Maps of the best filter combinations are shown in Figure 12. The spatial evaluation of filter efficiency is based on the signal homogeneity and amplitude preservation (see Equation 2).

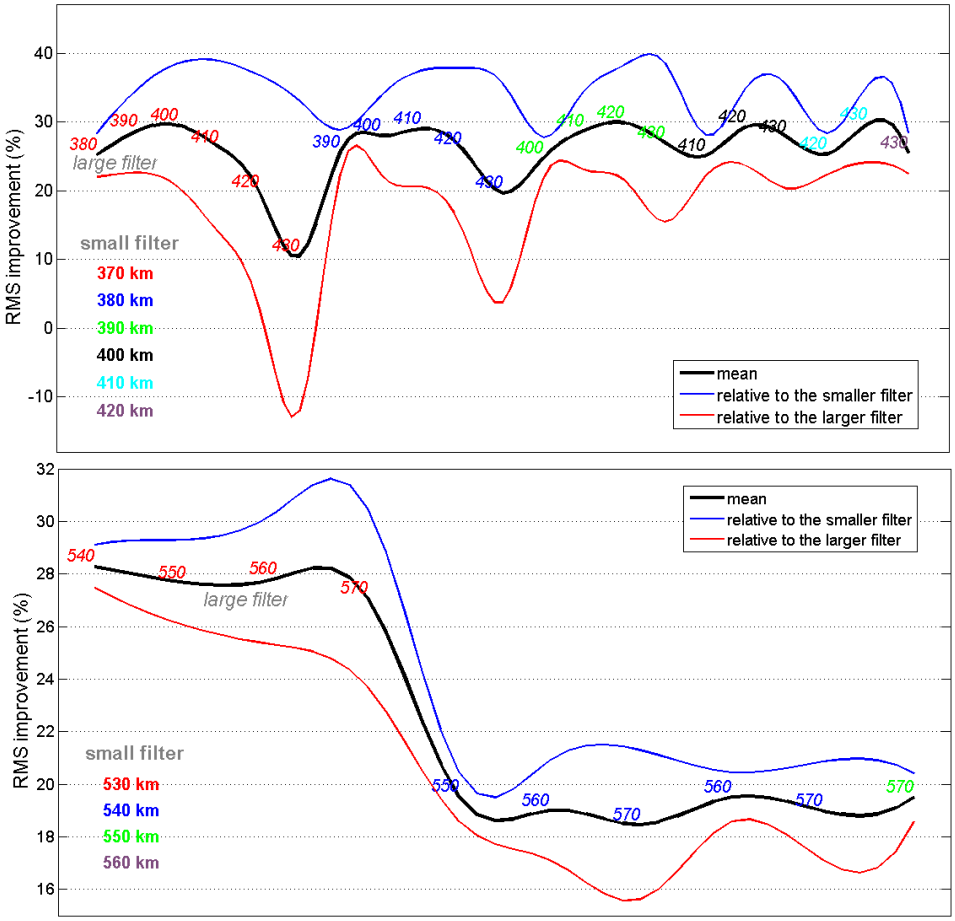

Figure 11) RMS improvement resulted from different combination of filter lengths applied based on seasonality for CS (upper plot) and Cg (lower plot).

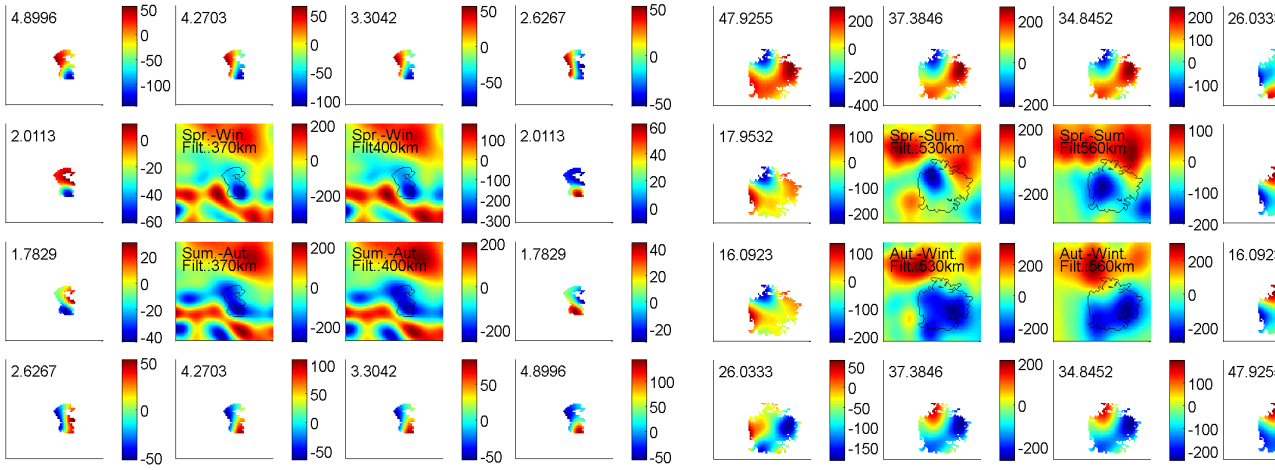

Figure 12. Seasonal filtering for CS (left) and Cg (right); the four inner cadres are filtered maps, and marginal cadres show the difference of tow aligned maps (i.e.: the closer map minus the farer one). RMS value of the difference maps are listed on the top of the cadres.

5 Discussion and Conclusions

Postprocessing of the gravimetry level-2 data usually consists on spatial filtering. Investigations on gravimetry filtering are concentrated on filter effects in the global scale, attempting to minimize the total global error. This is while, a specific filtering strategy which achieves good results on the global scale, might weakly perform in a local scale. Depending on the signal amplitude, globally optimized filters may obtain different results. For example, for high signal-to-noise ratio, such as interannual and smoothed signals, a strong DDK filter (e.g.: DDK4) perform well. However, for recovering low signal-to-noise ratios, strong DDK filters (DDK2 or DDK1) are needed.

The filtering process makes an improvement by removing correlated stripe-like errors in the data; however in the same time, a negative impact of filtering is that, it may also smooth the signal of interest. The smoothing rate depends on the filter strength. A filter that is weaker than the optimal filter necessary for a given study unit, lead to remaining the stripes; but a filter stronger than the optimal one, inversely, causes an uncompensable smoothing on interested signal. Therefore, it is essential to deliberate an optimum filter to make a balance between stripe removing and signal preserving. The most common confusion in the literature of the data postprocessing is that the filter induced error is mistakenly claimed to be compensated through scaling factors produced from auxiliary data, such as dominantly used hydrological models. This is while, any auxiliary data including hydrological models, are not capable to recover the distortions caused by spatial filtering. The claimed compensation in the literature, indeed, addresses only the SHT, and the geometry (i.e.: shape and area) effects,

rather than the filtering effect. Because, the smoothing process mixes spatially adjacent signals which are supposed to be unknown. Therefore, any negative side-effect of filtering will remain in the data as random errors, decreasing the final accuracy. The mean amplitude of these random errors increases with increase in the difference between the strengths of applied filter and the optimal one. For the purpose of filter effect recovering, hydrological models can be helpful provided that: 1- time series of scaling factors are produced rather than a single one; and more important, 2- the applied models are highly consistent with gravimetry data in terms of temporal and spatial resolutions; The second condition is definitely not met. Therefore, in terms of filter effect recovering, hydrological based scaling is not correct in single factor procedure, and not reliable in time dependent procedure. Furthermore, the fundamental assumption is that the satellite gravimetry data are more precise than common hydrological models in spatial and temporal dimensions (for the same parameters). Thus, relying on the hydrological models lead to inconsistency in the gravimetry derived results. Consequently, this is a wrong assumption in the literature, that the filtering side-effects would be recovered or decreased lately through data scaling. Conversely, the most focus should be applied on the filtering process itself in order to limit the filter negative effects. How much the filter is optimized, the filter induced errors would be limited.

The decorrelation methods can be classified on two categories: the first category approximates correlation error through a polynomial fitting, and then, subtracts it from the total signal. The second category reconstruct the data based on a *priori* information. The first category applies a realistic approach whereas they exploit statistics of data to spatially rectify the same data. However, they do not use the potential of any spatio-temporal patterns in the data. The second category, however, benefits from temporal patterns, although limited to a specific period (such as the month of August-2003 in DDK series). Several studies obtained a *priori* information from hydrological models; which may lead to result inconsistency as previously discussed. Those methods which use GRACE data to extract a *priori* information, such as DDK series, suffer from being static. They do not account for trends in satellite orbital information, neither for more possible, seasonal variations. The second category is, indeed, more than the common meaning for filters in image processing. This category exploits extra information over the signal to be filtered; they are thus, further than typical filters. By this definition, they function similar as 'correcting' or 'refining' tools, rather than 'filtering' tools.

In the present research, we benefit from the strength of the two filtering categories. We extract a *priori* information about the mass variations inside and outside the target area, from the GRACE data itself, in order to identify signal spatial gradient, which is employed to optimize a Poisson filter length. There is an inverse relationship between the slope of signal gradient and the optimal filter length. The benefit of this approach is the spatio-temporal dependency of optimal filter. Depending on signal spatial gradient, the optimal filter varies from one site to another. The spatial gradient may also vary in time, resulting

in change of the optimal filter length. For example, the long term change of signal gradient in the Greenland, where rate of Glacier melting has increased in last decades, has made it necessary to update the applied filter length. Dynamic filtering procedure is effective in minimizing filter induced error, in particular, for studying secular signals which is vulnerable to additive errors. The signal spatial gradient and thus respective optimal filter length may include seasonal cycle, e.g.: in the Caspian Sea and Congo River Basin.

The approach presented in this study adjust the balance between spatial destripping and signal smoothing. As only the isotropic Poisson filtering is investigated in this work, it worth to study anisotropic version of filters. The combination of characteristics of an anisotropic filter, and the time dependency specification presented in the current study, would result in a filtering strategy variable in time and space, which may develop the filter optimality, decreasing the filter-induced distortions.

Appendix A: Gravity signal propagation

Gravitation is a three-dimensional force that follows the Laplacain Equation to obtain total three-dimensional equilibrium. Gravity anomalies are represented by periodic functions. A combination of Fourier series (for longitudinal anomalies) and Associated Legendre Functions (for latitudinal anomalies) gives a Spherical Harmonic expansion. For any gravity change on the sphere, the lateral forces propagate radially with a pattern independent of anomaly's amplitude; depending on anomaly's SHT, XY position, and planar shape and geometry (Figure 13, left). Lord Rayleigh (1878) demonstrated that Bessel Functions are particular cases of Laplace Functions. On the base of the monomiality principle, it is possible to adapt Bessel Functions for Legendre polynomials (Abramowitz and Stegun, 1964; Cesarano and Ricci, 2016). Using the Legendre-Bessel connection, the radial signal propagations may be presented in the form of Bessel Functions of the Second Kind (Weber functions). It allows Legendre polynomials to be highly approximated in term of Bessel functions (Abramowitz and Stegun, 1964; Dattoli et al., 2003). Bessel's equation is defined by a differential equation (Equation 7),

$$x^2 \frac{d^2y}{dx^2} + x\frac{dy}{dx} + (x^2 - v^2)\, y = 0 \quad (7)$$

As a linear differential equation of second order has two solutions. The general solution is the Bessel functions, often presented in the form of integer order (Equation 8).

$$y = A\ J\nu(x) + B\ Y\nu(x) \quad (8)$$

where, $J\nu(x)$ and $Y\nu(x)$ are the Bessel function of the first and the second kinds respectively. The general form of Bessel's modified equation with n constant ( ), and its solution can be written as Equation 9 and Equation 10 respectively.

$$x^2 \frac{d^2y}{dx^2} + x\frac{dy}{dx} - (\beta^2 x^2 - v^2)\, y = 0 \quad (9)$$

$$y = C\ L\nu(\beta x) + D\ K\nu(\beta x) \quad (10a)$$

Supposing $\beta^2 = i$, where $i = \sqrt{-1}$

$$Y\nu(x)\frac{J\nu(x)*cos(\nu)-J_{-}\nu(x)}{\sin(\nu)} \quad (10b)$$

where $J(z)$ and $J_{-}(z)$ are a set of solutions of Bessel's equation.

$$J\nu(z) = \frac{Z}{2}^{v}\sum_{k=0}^{\infty}\frac{(\frac{-z^2}{4})^{k}}{k!\Gamma(v+k+1)} \quad (10c)$$

and $\Gamma(a)$ is the gamma function.

Bessel function of the second kind and order zero consist on infinite sinusoidal waves of fixed phase and decreasing amplitude. In gravity wave propagation the optimized Bessel-like function includes an additional term of a linear decrease in order to preserve orthogonality. The Bessel-like signal propagation are illustrated for SHT1 to SHT 100 in Figure 13 (right). The waves fluctuate in a decreasing manner, and the frequency increases with increase in SHT.

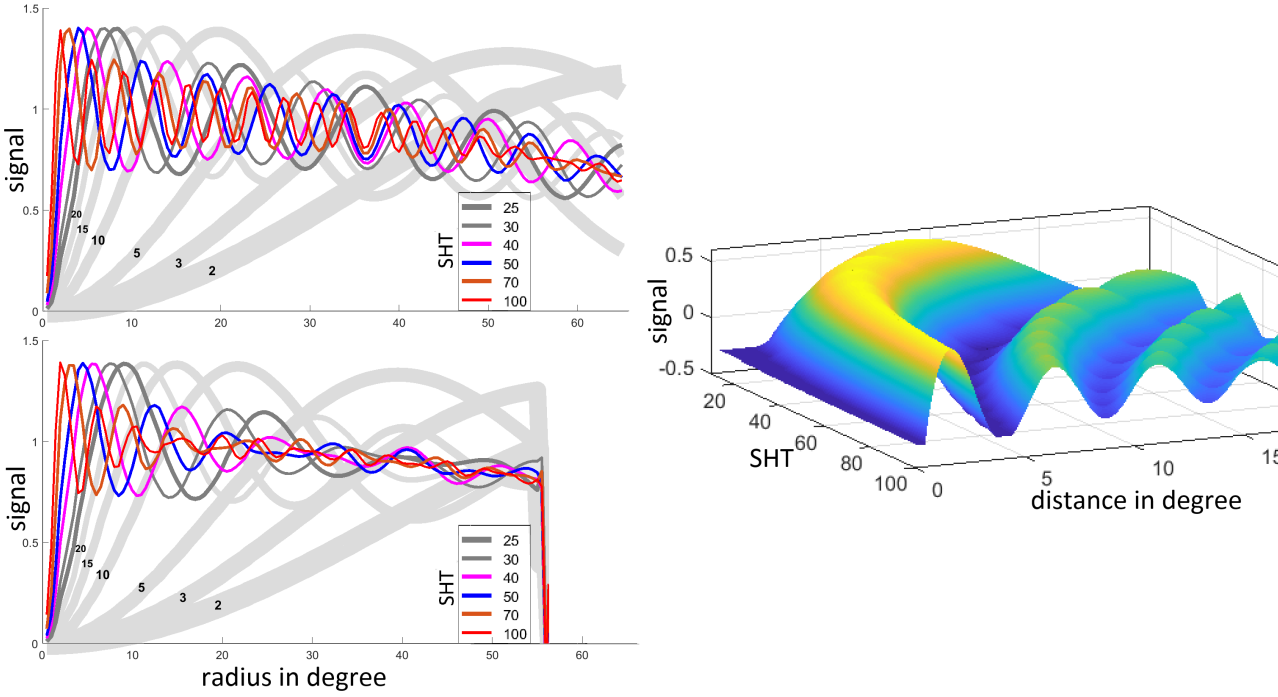

Figure 13. Spatial propagation of signal after expanding in different SHT, at Cg (upper right), and at CS (lower right); And the shapes of signal propagation based on the Bessel function for SHT 10 to 100 (left).

Acknowledgments

The author would like to acknowledge the GRACE-FO data provided by the JPL, from (http://grace.jpl.nasa.gov). GRACE-FO is a joint mission of the US

National Aeronautics and Space Administration and the German Research Center for Geosciences. The author appreciate Chro Hosseini for helps in optimizing some of the figures.

References

Abramowitz, M. & Stegun, I. (1964), Handbook of Mathematical Functions with Formulas, Graphs and Mathematical Tables. *United States department of Commerce, Library of Congress*.

Balaji, D. (2016), The effects of filtering on catchment scale GRACE solutions; *Water Resources Research*. DOI: http://dx.doi.org/10.1002/2016WR018960

Balaji, D. & Nico, S. (2017), The polar form of the spherical harmonic spectrum: implications for filtering GRACE data. *Journal of Geodesy*, DOI: http://dx.doi.org/10.1007/s00190-017-1037-7

Barletta, V.R., Sørensen, L.S. & Forsberg, R., (2013), Scatter of mass changes estimates at basin scale for Greenland and Antarctica. *Cryosphere, 7(5),* 1411–1432.

Baur, O., Kuhn, M., & Featherstone, W. E. (2009), GRACE-derived ice-mass variations over Greenland by accounting for leakage effects. *Journal of Geophysical Research-Solid Earth*, *114*, B06407, DOI: http://dx.doi.org/10.1029/2008JB006239

Bettadpur, S. (2007), Level-2 Gravity Field Product User Handbook; GRACE 327-734. *The GRACE Project, Center for Space Research, University of Texas at Austin*.

Cazenave, A., & Chen, J. (2010), Time-variable gravity from space and present-day mass redistribution in the Earth system. *Earth and Planetary Science Letters, 298(3-4)*, 263-274. DOI: http://dx.doi.org/10.1016/j.epsl.2010.07.035

Cesarano, C. & Ricci, E. (2016), The Legendre Polynomials as a basis for Bessel functions. *International Journal of Pure and Applied Mathematics; Volume 111 No. 1 2016,* 129-139, ISSN: 1311-8080 (printed version); ISSN: 1314-3395 (online version). Url: http://www.ijpam.eu. DOI: http://dx.doi.org/10.12732/ijpam.v111i1.12

Chambers, D. (2006), Analysis of Barotropic Sea Level Variations in the North Pacific Observed by GRACE. AGU Fall Meeting, San Francisco, CA; USA; 11-15 Dec. 2006, edited, *American Geophysical Union* 2000 Florida Ave NW Washington DC 20009-1277 USA URL: http://www.agu.org

Chen, J., C. Wilson, M. Rodell, and J. Famiglietti (2005), Low Degree Spherical Harmonic Influences on Basin-Scale Water Storage Change from GRACE, edited, p. 0035.

Chen, J. L., Rodell, M. Wilson, C. R. & Famiglietti, J. S. (2005), Low degree spherical harmonic influences on Gravity Recovery and Climate Experiment

(GRACE) water storage estimates. *Geophysical Research Letters, 32(14),* 14405, DOI: http://dx.doi.org/10.1029/2005GL022964

Chen, J.L., Wilson, C.R., Tapley, B.D., Blankenship, D.D., & Ivins, E.R. (2007), Patagonia Icefield melting observed by Gravity Recovery and Climate Experiment (GRACE). *Geophysical Research Letters, 34(22),* L22501.

Chen, J. L., Wilson, C. R., Tapley, B. D., Yang, Z. L., & Niu, G. Y. (2009), 2005 drought event in the Amazon River basin as measured by GRACE and estimated by climate models. *Journal of Geophysical Research-Solid Earth, 114*, B05404. DOI: http://dx.doi.org/10.1029/2008JB006056

Chen, J. L., Wilson, C. R., Blankenship, D., &. Tapley, B. D. (2009). Accelerated Antarctic ice loss from satellite gravity measurements. *Nature Geoscience, 2(12)*, 859-862. DOI: http://dx.doi.org/10.1038/ngeo694

Chen, J. L., Wilson, C. R., & Tapley, B. D. (2011), Interannual variability of Greenland ice losses from satellite gravimetry. *Journal of Geophyscal Researches; Solid Earth, 116*, 1–11. DOI: http://dx.doi.org/10.1029/2010JB007789

Chen, Q. J., Shen, Y. Z., Chen, W., Zhang, X. F., Hsu, H. Z., & Ju, X. L. (2015), A modified acceleration-based monthly gravity field solution from GRACE data. *Geophysical Journal International, 202(2),* 1190-1206. DOI: http://dx.doi.org/10.1093/gji/ggv220

DAT: The NASA GRACE Data Analysis Tool (DAT) provides 1x1 degree grids of water thickness derived from both GRACE and GRACE-FO (https://grace.jpl.nasa.gov/data-analysis-tool/).

Dattoli, G. (1999). Hermite Bessel and Laguerre; Bessel functions a by-product of the monomiality principle, in: D. Cocolicchio,

Dattoli, G., Srivastava, H. M. (Eds.) Advanced special functions and applications (Melfi, 1999), in: Proc. Melfi Sch. Adv. Top. Math., vol. 1, Rome, 2000, pp. 147164.

Dattoli, G., Srivastava, H. M.,and Sacchetti D. (2003), The Hermite polynomials and the Bessel functions from a general point of view; *International journal of Mathematics and Mathematical Sciences*. DOI: http://dx.doi.org/10.1155/s0161171203211133

Feng, G., Jin, S., & Sanchez Reales, J. M. (2013), Antarctic circumpolar current from satellite gravimetric models ITG-GRACE2010, GOCE-TIM3 and satellite *altimetry. Journal of Geodynamics, 72,* 72-80. DOI: http://dx.doi.org/10.1016/j.jog.2013.08.005

Feng, W., Zhong, M. and Xu H. (2012), Sea level variations in the South China Sea inferred from satellite gravity, altimetry, and oceanographic data; *Science China-Earth Sciences, 55(10),* 1696-1701. DOI: http://dx.doi.org/10.1007/s11430-012-4394-3

Fenoglio-Marc, L., J. Kusche, and M. Becker (2006). Mass variation in the Mediterranean Sea from GRACE and its validation by altimetry, steric and hydrologic fields; Geophysical Research Letters, 33(19), L19606, DOI: http://dx.doi.org/10.1029/2006GL026851.

Ferreira, L. G., S. Bettadpur, M. T. Coe, and M. H. Costa (2012). Water fluxes in the central Brazilian savanna: Seasonal patterns and land cover interdependencies as observed from GRACE, TRMM, and MODIS data; IEEE International Geoscience and Remote Sensing Symposium (IGARSS), 22-27July 2012, Munich, Germany, DOI: http://dx.doi.org/10.1109/IGARSS.2012.6352009.

Gardner, A. S., et al. (2013), A reconciled estimate of glacier contributions to sea level rise; 2003 to 2009; *Science, 340 (6134),* 852-857. DOI: http://dx.doi.org/10.1126/science.1234532

Guo, J., Dapeng, M., Xin, L., Haoming, Y., Zhongchang, S., Bin, B. (2016), Water Storage Changes over the Tibetan Plateau Revealed by GRACE Mission; *Acta Geophysica, 64(2),* 463-476. DOI: http://dx.doi.org/10.1515/acgeo-2016-0003

Gunter B., Ries, J., Bettadpur, S., Tapley B. (2006), A simulation study of the errors of omission and commission for GRACE RL01 gravity fields. *Journal of Geodesy, No 80.* DOI: http://dx.doi.org/10.1007/s00190-006-0083-3

Han, S. C., C. K. Shum, C. Jekeli, C. Y. Kuo, C. Wilson, and K. W. Seo (2005), Non-isotropic filtering of GRACE temporal gravity for geophysical signal enhancement. *Geophysical Journal International, 163(1),* 18-25. DOI: http://dx.doi.org/10.1111/j.1365-246X.2005.02756.x

Horvath A., Michael M., Roland P., and Martin H. (2018), Decorrelation of GRACE Time Variable Gravity Field Solutions Using Full Covariance Information. *Journal of Geosciences, 8, 323.* DOI: https://dx.doi.org/10.3390/geosciences8090323

Ince, E. S., Barthelmes, F., Reissland, S., Elger, K., Forste, C., Flechtner, F., & Schuh, H. (2019), ICGEM-15 years of successful collection and distribution of global gravitational models, associated services, and future plans; *Earth System Science Data, 11(2),* 647-674. 10.5194/essd-11-647.

Jacob, T., Wahr, J., Pfeffer, W. T., and Swenson, S. (2012), Recent contributions of glaciers and ice caps to sea level rise. *Nature, advance online publication, 514–518.* DOI: http://dx.doi.org/10.1038/nature10847

Jekeli, C. (1981), Alternative Methods to Smooth the Earth's Gravity Field. The Ohio State University, Columbus, OH, USA.

Jeon, T., Seo, K. W., Youm, K. et al (2018), Global sea level change signatures observed by GRACE satellite gravimetry. *Scientific Report 8,* 13519. https://doi.org/10.1038/s41598-018-31972-8

Johnson, G. C., and Chambers, D. P. (2013), Ocean bottom pressure seasonal cycles and decadal trends from GRACE release-05: Ocean circulation implications. *Journal of Geophysical Research: Oceans, 118(9),* 4228-4240. DOI: http://dx.doi.org/10.1002/jgrc.20307

Klees, R., Zapreeva, E. A., Winsemius, H. C. & Savenije, H. H. G. (2007), The bias in GRACE estimates of continental water storage variations. *Hydrology and Earth System Sciences Discussions. 3,* p. 3557-3594 38 p.

Klees, R., Revtova, E. A., Gunter, B. C., Ditmar, P., Oudman, E., Winsemius, H. C., and Savenije, H. H. G. (2008), The design of an optimal filter for monthly GRACE gravity models. *Geophysical Journal International, 175(2),* 417-432. DOI: http://dx.doi.org/10.1111/j.1365-246X.2008.03922.x

Koch, K. R., and Kusche J. (2002), Regularization of geopotential determination from satellite data by variance components. *Journal of Geodesy, 76(5),* 259. DOI: http://dx.doi.org/10.1007/s00190-002-0245-x

Kusche, J. (2007), Approximate decorrelation and non-isotropic smoothing of time-variable GRACE-type gravity field models. *Journal of Geodesy, 81(11),* 733-749. DOI: http://dx.doi.org/10.1007/s00190-007-0143-3

Kusche, J., Schmidt, R., Petrovic, S., and Rietbroek, R. (2009), Decorrelated GRACE time-variable gravity solutions by GFZ, and their validation using a hydrological model, *Journal of Geodesy, 83(10),* 903-913. DOI: http://dx.doi.org/10.1007/s00190-009-0308-3

Landerer, F. W., and Swenson, S. C. (2012), Accuracy of scaled GRACE terrestrial water storage estimates. *Water Resources Research, 48(4)*, W04531. DOI: http://dx.doi.org/10.1029/2011WR011453

Li, W., Zhang, C., Wen, H., Feng, W., Wang, W., Zhong, Y. (2019), The effects of leakage error on terrestrial water storage variations in the Yangtze River Basin measured by GRACE. *Journal of Applied Geophysics, 160,* 264-272. DOI: http://dx.doi.org/10.1016/j.jappgeo.2018.12.001

Long, D., Yang, Y., Wada, Y., Hong, Y., Liang, W., Chen, Y., Yong, B., Hou, A., Wei, J. and Chen L. (2015), Deriving scaling factors using a global hydrological model to restore GRACE total water storage changes for China's Yangtze River Basin; *Remote Sensing of Environment, 168,* 177-193. DOI: http://dx.doi.org/10.1016/j.rse.2015.07.003

Long, D., Longuevergne, L., and Scanlon, B. R. (2015), Global analysis of approaches for deriving total water storage changes from GRACE satellites; *Water Resources Research, 51(4),* 2574–2594. DOI: http://dx.doi.org/10.1002/2014WR016853

Longuevergne, L., Scanlon, B. R. and Wilson, C. R. (2010), GRACE hydrological estimates for small basins: Evaluating processing approaches on the High Plains aquifer, USA; *Water Resources Research, 46(11),* W11517, DOI: http://dx.doi.org/10.1029/2009WR008564

Lorenz (2009), Applying stochastic constraints on time-variable GRACE data; PhD Thesis, University of Stuttgart. DOI: http://dx.doi.org/10.13140/2.1.2719.3122

Luthcke, S. B. (2008), Recent land ice mass changes determined from satellite gravimetry. *Geological Society of America, 2008 annual meeting, Houston, TX, USA, United States,* Oct. 5-9, 2008, edited, p. 399, *Geological Society of America (GSA)* Boulder CO United States (USA), United States (USA).

Luthcke, S. B., D. D. Rowlands, J. J. McCarthy, H. J. Zwally, A. Arendt, D. K. Hall, and F. G. Lemoine (2008). Seasonal and Interannual Evolution of the Earth's Land Ice from GRACE MASCON Solutions; edited, p. 05, American Geophysical Union.

Maass, F., Martin, P., Olivares J., (2020), Analytic approximation to Bessel function J0(x). *Computational and Applied Mathematics, 39*: 222; https://dx.doi.org/10.1007/s40314-020-01238-z

Mu D., Yan, H., Feng W. and Peng P., (2017), GRACE leakage error correction with regularization technique: Case studies in Greenland and Antarctica; *Geophysical Journal International 208(3):*1775-1786. DOI: http://dx.doi.org/10.1093/gji/ggw494

Peng, P., Zhu, Y.-Z., Zhong, M., Yan, H.-M. and Kang K.-X., (2013), Annual sea level fingerprint caused by global water mass transport. *Chinese Journal of Geophysics-Chinese Edition, 56(3),* 824-833. DOI: http://dx.doi.org/10.6038/cjg20130311

Personal communication (August, 2020). Felix W. Landerer; GRACE Follow-On Project Scientist; Sea Level and Ice Group (329C); NASA Jet Propulsion Laboratory / California Institute of Technology.

Piecuch, C. G., Quinn, K. J. and Ponte, R. M. (2013), Satellite-derived interannual ocean bottom pressure variability and its relation to sea level. *Geophysical Research Letters, 40(12),* 3106-3110. DOI: http://dx.doi.org/10.1002/grl.50549

Piretzidis D. and Sideris, M. G. (2018), SHADE integrated software to apply empirical decorrelation on GRACE monthly SH. *Journal of Computers & Geosciences.*

Ramillien G., Seoane, L., Schumacher, M., Forootan, E., Frappart, F. and Darrozes, J. (2020), Recovery of Rapid Water Mass Changes (RWMC) by Kalman Filtering of GRACE Observations; *Journal of Remote Sensing, 12(8),* 1299. https://DOI.org/10.3390/rs12081299

Sasgen, I., van den Broeke, M., Bamber, J. L., Rignot, E., Sorensen, L. S., Wouters, B., Martinec, Z., Velicogna, I., and Simonsen, S. B. (2012), Timing and origin of recent regional ice-mass loss in Greenland. *Earth and Planet Scientific Letters, 333*, 293–303. DOI: http://dx.doi.org/10.1016/j.epsl.2012.03.033

Sasgen, I., Martinec, Z. and Fleming, K. (2006), Ice-mass loss in West Antarctica

from GRACE; AGU Fall Meeting; San Francisco, CA; USA; 11-15 Dec. 2006, edited, *American Geophysical Union 2000 Florida Ave NW Washington DC 20009-1277 USA* URL:http://www.agu.org

Sasgen, I., Martinec, Z., and Fleming, K. (2006), Wiener optimal filtering of GRACE data; *Studia Geophysica Et Geodaetica, 50(4),* 499-508. DOI: http://dx.doi.org/10.1007/s11200-006-0031-y

Schrama, E. J. O. and Wouters, B. (2011), Revisiting Greenland ice sheet mass loss observed by GRACE; *The journal of Geophysical Researches, Solid Earth, 116*, 1–10. DOI: http://dx.doi.org/10.1029/2009JB006847

Seoane, L., Ramillien, G., Frappart, F., and Leblanc, M. (2013), Regional GRACE-based estimates of water mass variations over Australia: validation and interpretation, *Hydrol. Earth System. Sciences., 17,* 4925–4939. DOI: https://doi.org/10.5194/hess-17-4925-2013

Shuanggen J. and Fang Z. (2015), Re-estimation of glacier mass loss in Greenland from GRACE with correction of land-ocean leakage effects. *Global and Planetary Change;* 2015; volume, pages 170-178.

Sorensen, L. S., Jarosch, A. H. Adalgeirsdottir, G. Barletta, V. R. Forsberg, R. Palsson, F. Bjornsson, H. and Johannesson, T. (2017), The effect of signal leakage and glacial isostatic rebound on GRACE-derived ice mass changes in Iceland; *Geophysical Journal International, 209(1),* 226-233. DOI: https://doi.org/10.1093/gji/ggx008

Swenson S, and Wahr J (2002), Methods for inferring regional surface-mass anomalies from Gravity Recovery and Climate Experiment (GRACE) measurements of time-variable gravity; *Journal of Geophysical Research B: Solid Earth.* 107: 3-1. DOI: http://dx.doi.org/10.1029/2001Jb000576

Swenson S and Wahr J (2002), Estimated effects of the vertical structure of atmospheric mass on the time-variable geoid. *Journal of Geophysical Research: Solid Earth. 107*: 4-1. DOI: http://dx.doi.org/10.1029/2000Jb00002

Swenson S., and Wahr J (2006), Post-processing removal of correlated errors in GRACE data; *Geophysical Research Letters. 33.* DOI: http://dx.doi.org/10.1029/2005Gl025285

Tang, J., Cheng, H. and Liu, L., (2012), Using nonlinear programming to correct leakage and estimate change from GRACE observation and its application to Antarctica, *Journal of Geophysical Research; 117*, B11410. DOI: http://dx.doi.org/10.1029/2012JB009480

Tangdamrongsub, N., Jasinski, M. F., & Shellito, P. J. (2021), Development and evaluation of 0.05 degrees terrestrial water storage estimates using Community Atmosphere Biosphere Land Exchange (CABLE) land surface model and assimilation of GRACE data, *Hydrology and Earth System Sciences, 25(7),* 4185-4208. DOI: https://doi.org/10.5194/hess-25-4185-2021

Tangdamrongsub, N., Hwang, C., Borak, J. S., Prabnakorn, S., & Han, J. C.

(2021), Optimizing GRACE/GRACE-FO data and a priori hydrological knowledge for improved global terrestial water storage component estimates, *Journal of Hydrology, 598.* https://doi.org/10.1016/j.jhydrol.2021.126463

Tapley, B.D., Bettadpur, S., Watkins, M.M., Reigber, C., (2004), The Gravity Recovery and Climate Experiment; Mission Overview and Early Results, *Geophysical Research Letters, 31 (9),* L09607, DOI: http://dx.doi.org/10.1029/2004GL019920

University of Wisconsin Madison (2011). The Nelson Institute for Environmental Studies: Center for Sustainability and the Global Environment SAGE: Research, no. WI.

Velicogna, I. (2009), Increasing rates of ice mass loss from the Greenland and Antarctic ice sheets revealed by GRACE; *Geophyscal Research Letter, 36,* 1–4. DOI: http://dx.doi.org/10.1029/2009GL040222

Velicogna, I., Sutterley, T. C. and van den Broeke, M. R. (2014), Regional acceleration in ice mass loss from Greenland and Antarctica using GRACE time-variable gravity data. *Geophysical Research Letters, 41(22),* 8130-8137. DOI: http://dx.doi.org/10.1002/2014gl061052

Velicogna, I., and Wahr, J. (2006), Acceleration of Greenland ice mass loss in spring 2004; *Nature, 443(7109),* 329-331. DOI: http://dx.doi.org/10.1038/nature05168

Wahr J, Molenaar, M., Bryan, F. (1998), Time variability of the Earth's gravity field: Hydrological and oceanic effects and their possible detection using GRACE. Journal of Geophysical Research: Solid Earth. *103:* 30205-30229. *DOI:* http://dx.doi.org/10.1029/98Jb02844

Willis, J.K., Chambers, D.P. & Nerem, R.S. 2008. Assessing the globally averaged sea level budget on seasonal to interannual time scales; J. geophys. Res., 113, C06015, DOI: http://dx.doi.org/10.1029/2007JC004517

Wiese, D. N., Yuan, D.-N., Boening, C., Landerer, F. W., Watkins, M. M. (2018), JPL GRACE Mascon Ocean, Ice, and Hydrology Equivalent Water Height Release 06 Coastal Resolution Improvement (CRI) Filtered Version 1.0. Ver. 1.0. PO.DAAC, CA, USA. DOI: http://dx.doi.org/10.5067/TEMSC-3MJC6.

Wouters, B., and Schrama, E. J. O. (2007). Improved accuracy of GRACE gravity solutions through empirical orthogonal function filtering of spherical harmonics; *Geophysical Research Letters, 34(23),* L23711, DOI: http://dx.doi.org/10.1029/2007GL032098

Zektzer, I. S., (1973), Studying the role of groundwater flow in water and salt balances of lakes; *the hydrology of Lakes, Helsinki Symposium,* IAHS Publ. 109, p. 197-201.

Zhong, M., Duan, J., Xu, H., Peng, P., Yan, H., and Zhu Y. (2009), Trend of China land water storage redistribution at medi- and large-spatial scales in

recent five years by satellite gravity observations. *Chinese Science Bulletin, 54(5),* 816-821. DOI: http://dx.doi.org/10.1007/s11434-008-0556-2

Zou, F., and Jin, S. (2014), Land-ocean leakage errors in satellite gravity measurements using forward modeling; *Third International IEEE Workshop on Earth Observation and Remote Sensing Applications (EORSA*), Changsha, China (2014.6.11-2014.6.14), 19–23. DOI: http://dx.doi.org/10.1109/EORSA.2014.6927841